Surface morphology of GaAs during molecular beam epitaxy growth: Comparison of experimental data with simulations based on continuum growth equations

A. Ballestad,* B. J. Ruck,† J. H. Schmid, M. Adamcyk, E. Nodwell, C. Nicoll,‡ and T. Tiedje
Department of Physics and Astronomy, University of British Columbia, Vancouver, BC V6T 1Z1, Canada
(Received 15 August 2001; revised manuscript received 29 November 2001; published 23 April 2002)

Using atomic force microscopy and *in situ* elastic light scattering we show that the surface of molecular beam epitaxy (MBE) grown GaAs tends towards an equilibrium roughness independent of the initial condition, as predicted by kinetic roughening theory. Two separate continuum growth equations are consistent with the observed equilibrium roughness, namely, the Kardar-Parisi-Zhang (KPZ) equation $\partial h/\partial t = \nu\nabla^2 h + (\lambda/2)\times(\nabla h)^2 + \eta$, where h is the surface height and η represents nonconservative noise, and the MBE equation $\partial h/\partial t = -\kappa\nabla^4 h - (\Lambda/2)\nabla^2(\nabla h)^2 + \eta_c$, where η_c represents conservative noise. These equations represent different physical smoothing mechanisms, so to distinguish between them we have numerically solved both equations. A novel geometric implementation of the nonlinear terms avoids instabilities associated with stiffness of the equations. We find that the time and length scale dependence of the smoothing of initially rough substrates is consistent with the KPZ equation but not the MBE equation. As the growth temperature is increased the coefficient ν increases relative to λ, but the KPZ description remains valid over the entire measured temperature range of 550–600 °C. Reducing the As overpressure increases the anisotropy of the surface morphology. We provide a physical interpretation of the KPZ equation in which the incorporation rate of mobile adatoms on the surface is governed by evaporation/condensation type dynamics. These results provide important insight into the MBE growth mechanism of GaAs.

DOI: 10.1103/PhysRevB.65.205302 PACS number(s): 68.55.−a, 81.10.Aj, 81.15.Aa

I. INTRODUCTION

A variety of important semiconductor devices are based on epitaxial thin films grown by techniques such as molecular beam epitaxy (MBE). In all of the important material systems, surfaces and interfaces play a fundamental role in determining the performance of these devices. The surfaces of growing films also provide a unique and interesting testing ground for a wide range of new theories and ideas relating to scale invariance in dynamical systems.[1–4] It is therefore crucial to understand the structure and evolution of the surface morphology during film growth.

GaAs homoepitaxy is a promising system in which to study the surface morphology of epitaxial films. However, a consistent description of the large scale properties of the grown surface is still lacking. This is partly due to the complexity introduced by the large number of growth parameters, such as the growth temperature, the arsenic overpressure, or the initial condition of the surface. One particularly useful tool for investigating the surface morphology of grown films is provided by continuum growth equations. Theoretical analysis of different growth mechanisms yields different continuum equations,[1–4] so determining the equation that best fits the experimental data can provide valuable insight into the dominant physical processes involved in the growth. For example, the presence of a Schwoebel barrier[5,6] that inhibits downward diffusion of mobile atoms at step edges leads to an unstable growth equation. Mounds observed on MBE grown GaAs surfaces[7–12] have in some cases been attributed to this phenomenon.[7–10]

More recently, we have used a stable growth equation, namely, the Kardar-Parisi-Zhang (KPZ) equation,[13] to show that mounds observed on GaAs grown at 550 °C are actually a transient remnant of the rough initial surface.[14] The KPZ equation is nonconservative, that is, the growth rate of the surface depends on the local slope, a feature that is inconsistent with usual MBE growth conditions. For this reason a fourth order conservative growth equation (the MBE equation) has also been proposed,[15–17] in which smoothing occurs via surface diffusion. Determining which of these two equations best describes the evolving GaAs surface remains an outstanding issue.

In this paper we compare detailed real-time and *ex situ* measurements of MBE grown GaAs surfaces with numerical simulations of both the KPZ and the MBE equations. The KPZ equation with nonconservative noise quantitatively reproduces the observed surface morphology at all growth times over the entire measured range of spatial frequencies. The MBE equation with conservative noise predicts the correct long-time surface roughness, but cannot account for the smoothing rate of large scale surface features. We therefore conclude that GaAs homoepitaxy is described by the KPZ equation. To account for the nonconservative nature of the KPZ equation we introduce a simple, physically realistic normalization scheme for the growth rate, although for our surfaces this modification has very little effect on the results.

II. CONTINUUM GROWTH EQUATIONS

In a continuum approximation, where the discrete nature of the atoms is averaged out, the evolution of the surface morphology during film growth can be described by a continuum growth equation. In this approach the time rate of change in the surface height $h(\mathbf{x},t)$ is expressed in terms of the various derivatives of h.[1–4]

A. Kardar-Parisi-Zhang equation

One of the most studied continuum equations is the KPZ equation[13]

$$\frac{\partial h}{\partial t} = \nu \nabla^2 h + \frac{\lambda}{2}(\nabla h)^2 + \eta, \tag{1}$$

where $\eta = \eta(\mathbf{x},t)$ represents the random noise associated with the deposition and incorporation of atoms on the surface. Generally, the noise is assumed to be uncorrelated, with $\langle \eta(\mathbf{x},t)\,\eta(\mathbf{x}',t')\rangle = D\,\delta(\mathbf{x}-\mathbf{x}')\,\delta(t-t')$, where $\langle \cdots \rangle$ represents an average over possible noise configurations. Physically, the linear term is used to represent evaporation/condensation dynamics between a vapor with a constant chemical potential μ_v and a surface with an average chemical potential $\mu_0 < \mu_v$. In the continuum approximation μ_0 is determined by the surface tension σ_s (free energy per unit surface area). To lowest order, variations about μ_0 are induced by the local surface curvature[1] as $\mu(\mathbf{x}) = \mu_0 - \sigma_s \nabla^2 h(\mathbf{x})$. The incorporation rate is determined by the relaxation ansatz $\partial h/\partial t = -\Upsilon \mu$, where $\Upsilon > 0$ is the interface mobility. Inserting the expression for μ and subtracting the constant growth rate $\Upsilon \mu_0$ yields the second order linear growth equation, with $\nu = \sigma_s \Upsilon$.

The nonlinear term is an approximation which is often used to model the situation where growth proceeds outward from the local surface normal,[1,2] although we show below that other interpretations are possible. It should be noted that the nonlinear term violates mass conservation as it does not conserve the average height of the surface. The KPZ equation with $\lambda = 0$ is often referred to as the Edwards-Wilkinson (EW) equation.[18]

B. MBE equation

Under typical GaAs MBE growth conditions, atoms arriving at the surface undergo significant diffusion before incorporating at favorable sites. If the sticking coefficient is unity then the growth rate is determined solely by the flux, and nonconservative terms should not be present in the growth equation. To this end the MBE equation has been formulated:[1,2,15–17,19,20]

$$\frac{\partial h}{\partial t} = -\kappa \nabla^4 h - \frac{\Lambda}{2}\nabla^2[(\nabla h)^2] + \eta, \tag{2}$$

where η may be either nonconservative flux noise with the correlation function defined above, or conservative diffusive noise with correlation function[1] $\langle \eta(\mathbf{x},t)\,\eta(\mathbf{x}',t')\rangle = D_c \nabla^2 \delta(\mathbf{x}-\mathbf{x}')\,\delta(t-t')$. The fourth order linear term can be derived from a conservation law, in which surface currents are driven by gradients in the surface chemical potential.[1,21] The fourth order nonlinear term is believed to be generated by a nonequilibrium surface chemical potential induced by the deposition flux.[1] Note that we neglect the term $\nabla(\nabla h)^3$ as no physical mechanism is known to generate this term in the absence of the $\nabla^2 h$ term.[17]

C. Conservative KPZ equation

A conservative version of the KPZ equation can be generated by modifying the nonlinear term. To achieve this, we first note that when the growth proceeds outward from the surface normal at a constant rate λ, the growth rate can be projected onto the vertical direction leading to

$$\frac{\partial h}{\partial t} = \lambda \sqrt{1+(\nabla h)^2} \approx \lambda \left[1 + \frac{1}{2}(\nabla h)^2 \right], \tag{3}$$

demonstrating the link between normal growth and the KPZ term. The approximation is valid for $|\nabla h| \ll 1$. For a rough surface of side length L, Eq. (3) leads to the addition of a total volume

$$\delta V = \delta t \int_0^L \lambda \sqrt{1+(\nabla h)^2}\, d^2\mathbf{x},$$

$$= \lambda\, \delta t L^2 \langle \sqrt{1+(\nabla h)^2} \rangle, \tag{4}$$

in an infinitesimal time δt, where $\langle \cdots \rangle$ represents an average over the surface. On a perfectly flat surface of the same dimensions the total volume added is simply $\delta V_0 = \lambda\, \delta t L^2$. A conservative growth equation is obtained by normalizing the volume added, then subtracting the growth rate. This is achieved through the substitution

$$\frac{\lambda}{2}(\nabla h)^2 \rightarrow \lambda \left[\frac{\delta V_0}{\delta V} \sqrt{1+(\nabla h)^2} - 1 \right], \tag{5}$$

where we have used the approximation in Eq. (3). Physically, in the case of GaAs growth discussed here, the correction describes the situation where the density of mobile atoms on the surface adjusts itself such that the net incorporation rate balances the arrival rate of atoms from the growth flux. The resulting equation is nonlocal, and is difficult to investigate using standard analytical techniques. However, it is easy to simulate the behavior numerically, as we show below. Hereafter, unless specifically stated, all references to the KPZ equation refer to the conservative version which is consistent with the physical process of MBE growth.

D. Universality classes

The different kinds of growth process, as represented by the different growth equations, can be characterized by their universality class. Associated with each universality class is a set of exponents α (roughness exponent), β (growth exponent), and $z \equiv \alpha/\beta$ (dynamic exponent), describing the scaling properties of the surface. Table I summarizes the known exponents for some of the growth equations.[2]

Experimental measurements of the surface shape can be used to extract the growth exponents, thereby giving an indication of the particular equation governing the surface evolution. One useful measure is the power spectral density (PSD), defined by

$$\mathrm{PSD}(\mathbf{q},t) = [\hat{h}(\mathbf{q},t)]^2, \tag{6}$$

TABLE I. Critical exponents associated with various growth equations in $(2+1)$ dimensions. The second column indicates whether the noise is conservative (C) or nonconservative (N).

Equation	Noise	α	β	z
EW	N	0	0	2
KPZ	N	0.385	0.24	1.58
MBE	N	0.667	0.2	3.333
MBE	C	0	0	4

where $\hat{h}(\mathbf{q},t)$ is the Fourier transform of $h(\mathbf{x},t)$ at spatial frequency $\mathbf{q}$. After a long period of growth the PSD is expected to approach an asymptotic form determined by the critical exponents of the growth equation. In $(2+1)$ dimensions the asymptotic form is $\mathrm{PSD}(t\rightarrow\infty)\sim q^{-2(1+\alpha)}$, where $q=|\mathbf{q}|$, and the overall amplitude depends on both the strength of the noise and the coefficients in the growth equation. For finite growth times, the asymptote will be observed only for q larger than some cutoff value $q_c\sim t^{-1/z}$.

E. Simulations

The critical exponents given in Table I for the different growth equations are difficult to determine experimentally, due to a limited dynamic range accessible during growth. Furthermore, for real systems the morphology of the starting surface may also affect the scaling properties of the system at finite growth times. During this transient regime, measurements of the scaling exponents may not reveal the universality class. Instead, it is desirable to compare the measured surfaces to simulations of the different growth equations.

We have discretized the continuum growth Eqs. (1) and (2), including the modification described by Eq. (5). Numerical instabilities restrict the range of parameters which can be used in typical finite difference implementations of the nonlinear terms,[22] so instead we have used a novel implementation based on the normal growth approximation to the KPZ term [Eq. (3)]. The algorithm translates all points on the surface outwards from the normal by a constant amount, thereby providing an excellent way to approximate the $(\nabla h)^2$ term. Details of the implementation of this term and the other terms in the growth equation are provided in the Appendix.

Nonconservative noise is included in the simulations by adding an amount $\Gamma_n\sigma_n\sqrt{12\Delta t}U(t)$ to each point on the surface at each time step,[2] where $\sigma_n^2=2D/(\Delta x)^2$, Δx is the spacing between the lattice points in the simulation, Δt is the simulation time step, $U(t)$ is a random number uniformly distributed between -0.5 and 0.5, and Γ_n is a dimensionless fitting parameter. For flux noise, one expects $\Gamma_n=1$, and $D=Fa^3$ in our units,[2] where F is the flux in nm/s, and a is the GaAs monolayer height (0.28 nm).

Conservative noise can also arise during the growth process due to fluctuating currents of adatoms flowing on the surface. We have implemented an algorithm to approximate conservative noise in the following way. At each time step, we add/remove an amount $\Gamma_c\sigma_c\sqrt{12}U(t)$ from each point on the surface and transfer exactly this amount to one of the nearest neighbor sites. This is repeated for each of the four nearest neighbors, using periodic boundary conditions. The coefficient $\sigma_c=\sqrt{\Delta t/(\Delta x)^4}$ ensures that the amplitude of the PSD generated by the simulations does not change if we vary the lattice spacing Δx or time step Δt. Γ_c is a fitting parameter with dimensions $\mathrm{nm}^3/\mathrm{s}^{1/2}$ that adjusts the overall noise level to optimize the match between the simulations and experimental data. Generally, Γ_c is expected to increase as either the number of mobile atoms or the individual adatom diffusion constant increases. Although other, more detailed implementations of conservative noise are certainly possible, our algorithm is adequate for testing the continuum growth equations.

Simulations of each of the growth equations described above have been used to generate the PSD at a range of different times, using a flat surface as the initial condition. The fourth order MBE equation was simulated using either conservative or nonconservative noise. In all cases the critical exponents extracted from the PSDs agree within uncertainty with the values given in Table I, confirming the accuracy of our numerical schemes.

III. EXPERIMENTAL METHOD

All samples in this study were prepared on [001] oriented GaAs substrates in a VG-V80H MBE chamber equipped with solid source effusion cells for both group III and group V elements. The growth rate, determined by the Ga flux, was kept constant at around 1 μm/h during each run. A valved cracker was used as the As source, under conditions which give almost entirely As_2 as the group V flux. The group V to group III beam equivalent pressure (BEP) flux ratios were estimated from measurements made with an ion gauge placed in front of the samples. The substrate temperature was monitored by optical bandgap thermometry[23] throughout the growth, with an absolute accuracy of about $\pm 5\,^{\circ}\mathrm{C}$. Prior to loading into the MBE chamber, the substrates were exposed to ultraviolet ozone to remove carbon contaminants. The resulting surface oxide was removed *in situ*, either by thermal evaporation at $600\,^{\circ}\mathrm{C}$ under an As_2 overpressure, or by an atomic hydrogen etch. The hydrogen used in the etch was cracked with a W filament placed in front of the sample. During the etch the substrate was nominally set to $150\,^{\circ}\mathrm{C}$, but radiation from the W filament caused the temperature to rise somewhat above this value. Details of the parameters associated with each sample can be found in Table II.

During growth, the surface roughness was monitored by elastic light scattering. Light from a chopped Hg arc lamp was incident through a quartz viewport onto the growing sample. The surface roughness diffusely scatters some of the incident light out of the chamber through two additional viewports, where it is detected by photomultiplier tubes fitted with wavelength selective filters. The chamber geometry, and the wavelength of light monitored, allows us to measure the roughness at spatial frequencies of 16 and 41 $\mu\mathrm{m}^{-1}$, corresponding to length scales of 393 and 153 nm, respectively. In fact, it can be shown that the measured light scattering signal is proportional to the PSD of the surface at the spatial fre-

TABLE II. Summary of growth parameters for the samples described in the text. T_{sub} is the substrate temperature and V:III is the Ga to As flux ratio (BEP) during growth. The oxide removal method is either thermal desorption (TD) or hydrogen etch (HE).

Sample	T_{sub} (°C)	Growth time (min)	V:III	Surface prep.
730 T0		0		TD
744 H1	595	75	6.5	HE
755 T4	550	75	2.9	TD
769 H0		0		HE
776 H2	552	10	5.5	HE
780 H3	553	37.5	6.5	HE
836 T6	600	69	8.3	TD
838 T2	550	37.5	7.8	TD
839 T1	550	10	8.3	TD
841 T3	550	150	8.4	TD
852 T5	550	3	8.5	TD
899 H5	550	30	1.0	HE
912 H4	550	30	3.0	HE

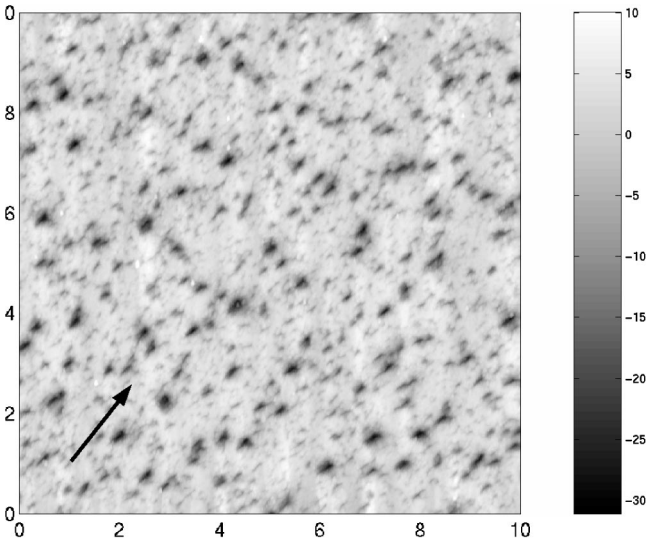

FIG. 1. A 10×10 μm^2 AFM image of a GaAs wafer after thermal removal of the surface oxide (sample $T0$). The scale bar is in nm, and the arrow points along the $[1\bar{1}0]$ direction.

quency monitored.[24,25] The scattering vectors for the two signals are 22.5° apart on the plane of the wafer, so the roughness is probed along slightly different directions on the film surface.

Atomic force microscope (AFM) images were obtained from the samples soon after removal from UHV, using a Digital Instruments Multimode Scanning Probe Microscope. Scans ranging from 1×1 μm^2 to 100×100 μm^2 were taken in tapping mode using Si tips with approximate tip radius 30 nm.[26] Therefore, we can obtain reliable data up to spatial frequencies of at least 100 μm^{-1} before tip convolution effects become significant.

IV. RESULTS AND ANALYSIS

A. Growth on thermally desorbed substrates

1. Time dependence

Figure 1 shows a GaAs surface immediately prior to growth, after thermal cleaning of the surface oxide. The thermal desorption process produces a surface covered with pits, with the largest pits separated by a characteristic distance of around 1 μm, and having a maximum depth of around 40 nm. Figure 2 shows a set of AFM scans from samples grown for different times at 550 °C on thermally cleaned substrates, using a similar As_2 flux for each growth. Each of the grown surfaces is covered with mounds elongated along the $[1\bar{1}0]$ crystal axis, and separated by sharp V grooves. The mounds have a characteristic separation similar to that of the pits on the starting surface, strongly suggesting that they are a remnant of the initial condition.

The r.m.s. roughness of the surfaces shown in Figs. 1 and 2 decreases steadily with time during growth, progressing through 4.9, 1.0, 0.7, and 0.5 nm after 0, 10, 37.5, and 150 min of deposition, respectively. This smoothing is inconsistent with the ideas of unstable growth,[9,10] in which the mounds would be expected to increase in amplitude as time progresses. A careful comparison of Figs. 2(a)–2(c) shows also that the number of mounds decreases as the surface smooths, while the lateral length scale of the remaining mounds increases. This is consistent with the behavior expected from the second order nonlinear term in Eqs. (1) and (5); the mounds grow outward in time such that the larger mounds absorb the smaller ones.

If a single continuum equation is to be used to describe the surface evolution, then the equation must be capable of reproducing the morphology after a range of different growth times. The persistence of V grooves on the surface suggests that a nonlinear equation, such as the KPZ or MBE equations, is the correct choice. Figure 3 shows two surfaces simulated using the KPZ equation with parameters $\nu_x = 10$ nm^2/s, $\nu_y = 1$ nm^2/s, and $\lambda_x = \lambda_y = 12$ nm/s, where the subscripts x and y correspond to the $[1\bar{1}0]$ and $[110]$ directions, respectively. Nonconservative noise was included in each of the simulations with strength $\Gamma_n = 10$, considerably larger than the value $\Gamma_n = 1$ expected from the random arrival of atoms from the flux (see Sec. II E). Figure 4 shows two surfaces simulated using the MBE equation with parameters $\kappa_x = 3\times10^5$ nm^4/s, $\kappa_y = 10^5$ nm^4/s, $\Lambda_x = 10^6$ nm^3/s, and $\Lambda_y = 10^5$ nm^3/s. Conservative noise was added to these simulations with strength $\Gamma_c = 100$ nm^3/s$^{1/2}$. In both cases the simulations are performed on a 256×256 grid, using an AFM scan of the desorbed wafer as the initial condition.

For both sets of simulations the times match the shortest two growth times in Fig. 2 (10 and 37.5 min), and the coefficients have been adjusted to provide the best possible agreement with the experimental data. Note that the coefficients used for the KPZ simulations are slightly different to those used in Ref. 14 to model a 75 min growth. This is due to slight variations in the surface morphology caused by the higher As_2 overpressure used during the growth of the present samples. Without the nonlinear terms both growth

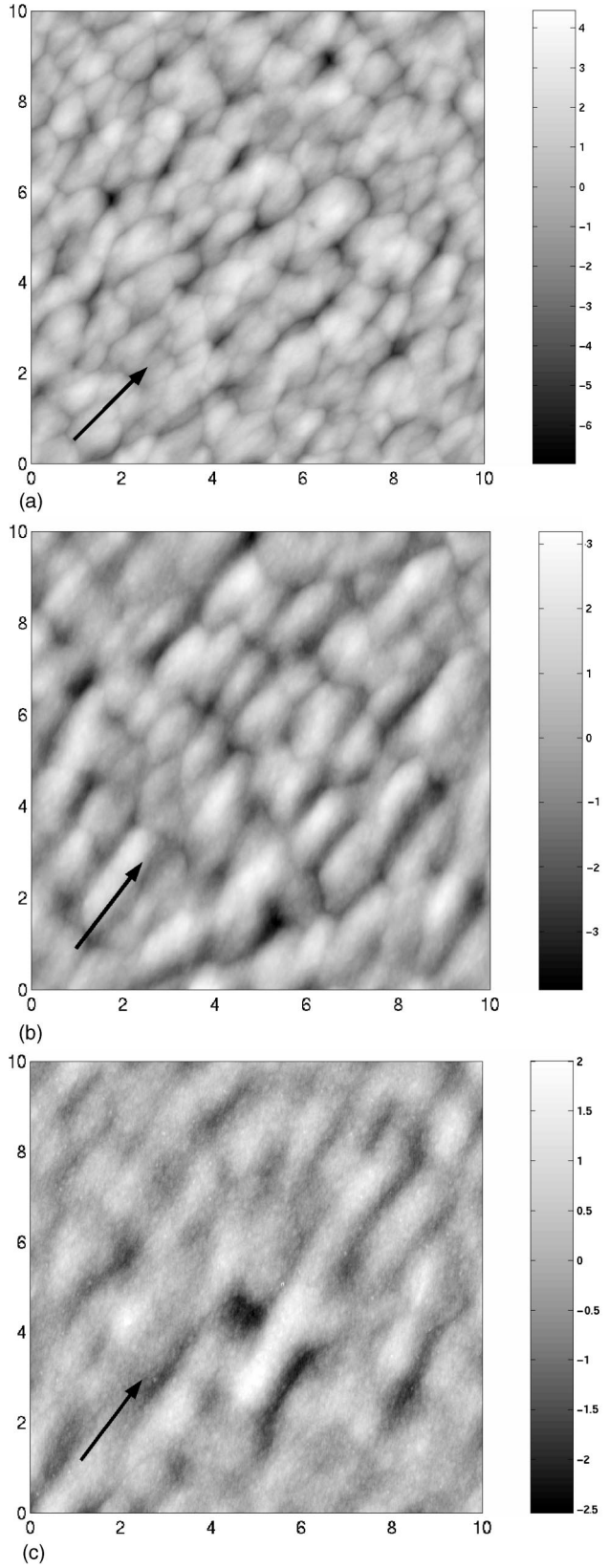

FIG. 2. 10×10 μm^2 AFM images from samples grown under nominally identical conditions, but for different times, on thermally desorbed substrates. (a) 10 min growth (sample $T1$). (b) 37.5 min growth (sample $T2$). (c) 150 min growth (sample $T3$). The scale bars are in nm, and the arrows point along the $[1\bar{1}0]$ direction.

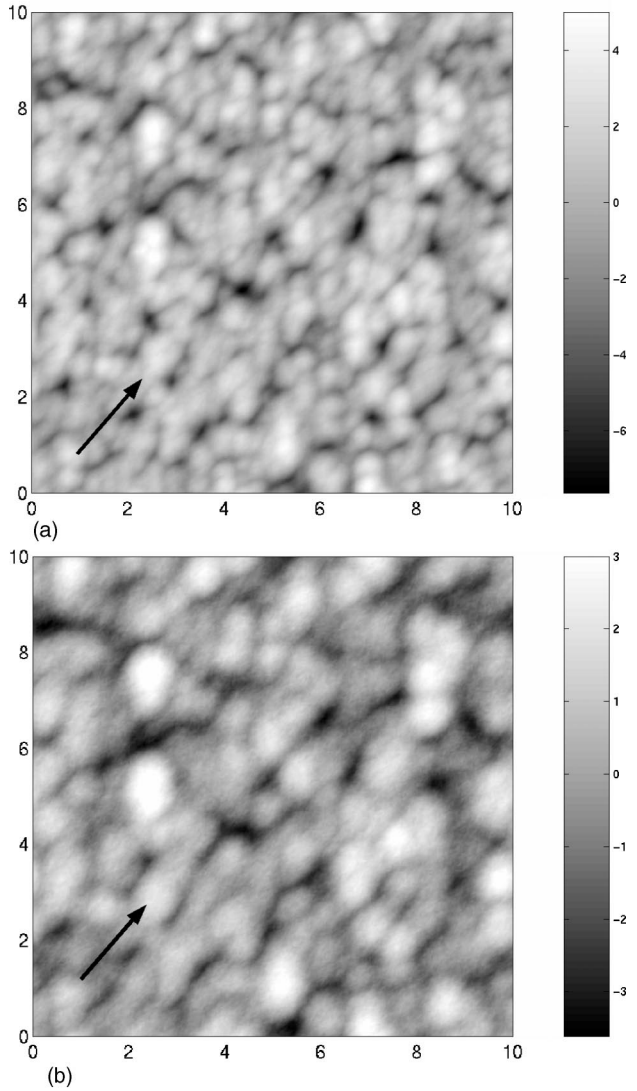

FIG. 3. 10×10 μm^2 simulations generated using the conservative form of the KPZ equation with growth times of (a) 10 min and (b) 37.5 min. The scale bars are in nm, and the arrows point along the $[1\bar{1}0]$ direction. The simulations compare well with the real surfaces shown in Fig. 2.

equations generate inversion symmetric surfaces,[1–4] whereas with our inclusion of the nonlinear terms both equations cause the etch pits on the starting surface to develop into mounds separated by V grooves, in agreement with the experimental surface morphology. However, while the surfaces generated by the KPZ equation have similar roughness to the real surfaces at all length scales, the MBE equation generates less smoothing of the largest features than is seen in the experiment. Modifying the parameters of the MBE equation to enhance smoothing of the deepest pits causes the smaller mounds to be less prominent than those on the real surface.

Figure 5(a) shows the PSDs of a thermally desorbed substrate (sample $T0$), a sample grown for 10 min (sample $T1$), and a sample grown for 150 min (sample $T3$), measured along the $[1\bar{1}0]$ direction. Figure 5(b) shows the PSD from the same surfaces measured along the $[110]$ direction. PSDs

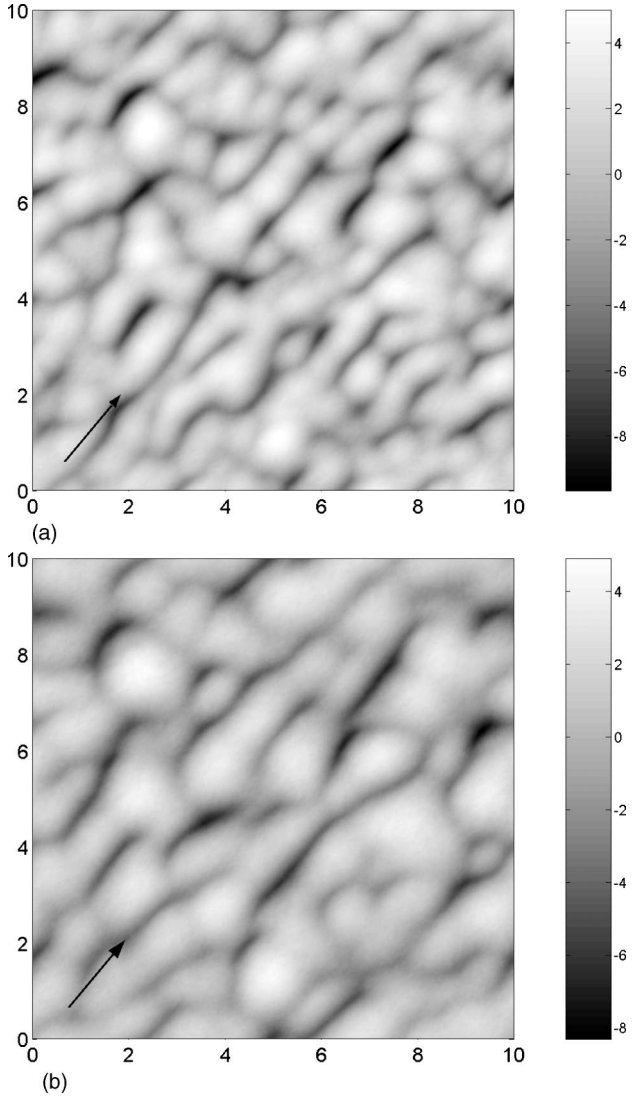

FIG. 4. 10×10 μm^2 simulations generated using the MBE equation with growth times of (a) 10 min and (b) 37.5 min. The scale bars are in nm, and the arrows point along the $[1\bar{1}0]$ direction. The fourth order equation also produces a mounded surface, although the depth of the cusps between the mounds is greater than on the real surfaces.

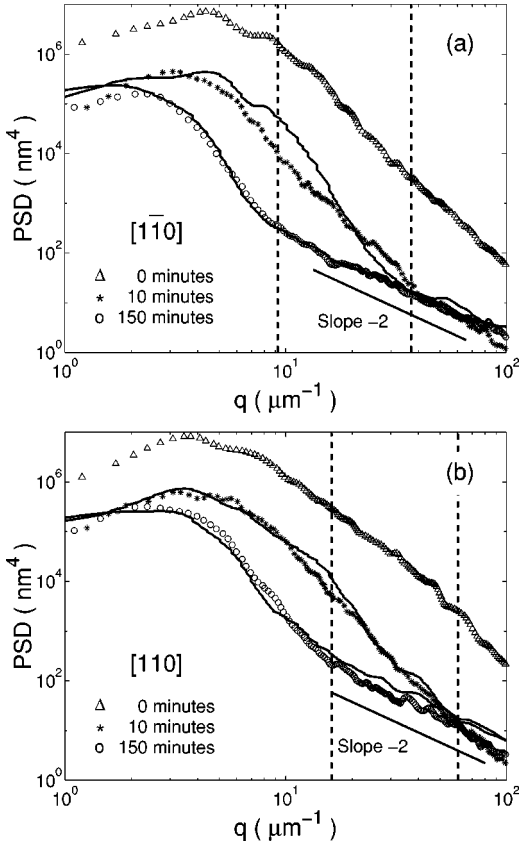

FIG. 5. PSD after different growth times on thermally cleaned substrates, measured along (a) the $[1\bar{1}0]$ direction and (b) the $[110]$ direction. The symbols represent the experimental data. The solid lines, representing 10 and 150 min simulations generated with the KPZ equation, are in excellent agreement with the experimental data. The vertical dashed lines indicate the cutoff frequencies q_c at 10 and 150 min (right to left).

calculated from AFM scans ranging in size from 1 $\times1$ μm^2 to 100×100 μm^2 were combined to generate these figures. The PSD shrinks rapidly as a function of time during growth, until it reaches a saturated level for spatial frequencies greater than a crossover frequency q_c (indicated by the vertical dashed lines). The crossover frequency decreases monotonically as a function of growth time, going from around 36 μm^{-1} to around 9 μm^{-1} ($[1\bar{1}0]$ direction), or from around 60 μm^{-1} to around 17 μm^{-1} ($[110]$ direction) after 10 and 150 min growth, respectively. In the saturated region ($q>q_c$) the PSD is well described by a power law, with slope close to -2, and a magnitude which is the same for all samples grown under similar conditions. The peak in the PSD of the thermally desorbed surface, located at around 4 μm^{-1}, moves gradually towards lower spatial frequencies during growth as the average size and spacing of the mounds increases.

The solid lines on Fig. 5 show the PSD's obtained from simulations using the conservative form of the KPZ equation. Figure 6 shows the PSD of the same samples shown in Fig. 5, but in this case the solid lines are PSDs obtained from simulations using the MBE equation. The simulation times match the experimental data, and the parameters are the same as those used to generate the images shown in Figs. 3 and 4. As above, the PSD's are generated from a combination of simulated surfaces of different sizes. In the saturated region $q>q_c$ the magnitude of the PSD is determined by both the coefficients in the growth equation and the strength of the noise included in the simulations. The values of the parameters Γ_n (KPZ equation) and Γ_c (MBE equation) quoted above were determined by matching the simulated and measured PSD's in the saturated region at high spatial frequencies.

The KPZ simulations in Fig. 5 are in excellent agreement with the experimental data over the entire q range. For $q>q_c$ the MBE equation with conservative noise predicts the correct slope on the log-log plot (Fig. 6). However, unlike the KPZ equation, it does not predict the time dependence of

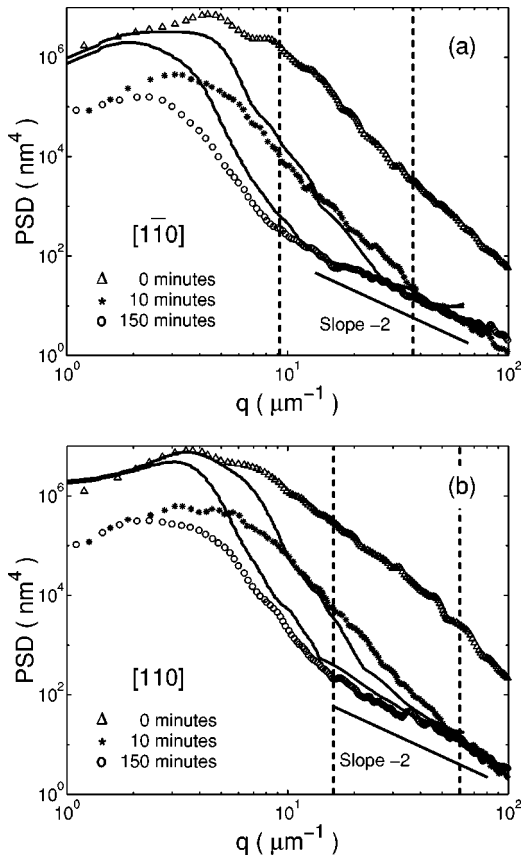

FIG. 6. PSD of the same samples shown in Fig. 5, measured along (a) the $[1\bar{1}0]$ direction and (b) the $[110]$ direction. The solid lines are from 10 and 150 min simulations generated with the MBE equation. The simulated PSD has a stronger q dependence than the PSD of the grown films. The vertical dashed lines indicate the cutoff frequencies q_c at 10 and 150 min (right to left).

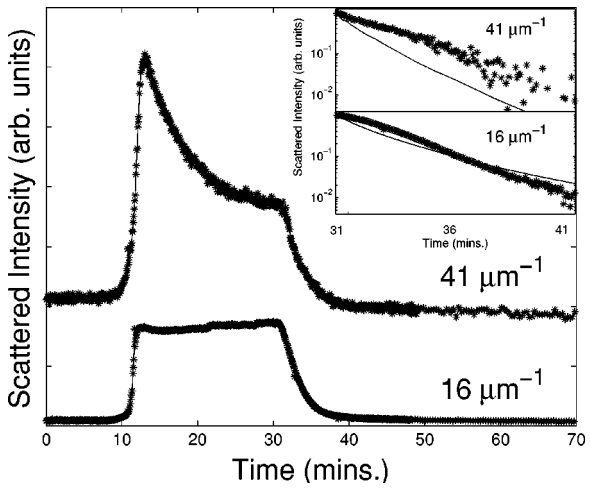

FIG. 7. Diffuse light scattering signal at 16 and 41 μm^{-1} measured during growth of sample $T4$. For clarity, the 41 μm^{-1} signal has been offset. The insets show semilogarithmic plots of portions of the same data during the growth, after subtraction of the constant background level. The solid lines on both plots show the predicted light scattering from simulations using the KPZ equation.

the cutoff frequency, and for $q<q_c$ it tends to predict a slope steeper than the experimental data. Very little smoothing takes place at the lowest spatial frequencies in the MBE equation simulations, whereas the experimental data clearly show a decrease corresponding to filling in of the thermal desorb pits.

The time dependence of the surface roughness can also be monitored by elastic light scattering. Figure 7 shows the measured light scattering signal at spatial frequencies of 16 and 41 μm^{-1} during the thermal cleaning and subsequent growth of sample $T4$. AFM images from this sample have been published previously.[14] The thermal desorption of the surface oxide at 600 °C, which takes place at around 10 min in the figure, is accompanied by a rapid increase in the scattered light intensity at both spatial frequencies, caused by the appearance of the desorption pits seen in Fig. 1. The sample is maintained at 600 °C for several minutes to complete the oxide removal, during which time the surface smooths considerably at 41 μm^{-1} but stays approximately constant at 16 μm^{-1}, corresponding to the annealing of some short scale features. The sample is brought down to growth temperature (550 °C) after 23 min, and growth begins at a time of 31 min. The surface immediately begins to smooth at both length scales, until a background level is reached after about 10 min of growth.

The light scattering data indicate that, during growth, the surface smooths at a rate which is approximately independent of the probed length scale. In fact, the data are well described by an exponential decay with time constants τ_{16} and τ_{41} both equal to around 3 min. An exponential decay would be expected from purely linear equations such as the EW equation or the fourth order linear term in the MBE equation. However, the EW equation predicts the characteristic smoothing times to be in the ratio $\tau_{41}/\tau_{16}=(16/41)^2$, and the linear MBE equation predicts the ratio $(16/41)^4$, both inconsistent with the observed ratio.

The predicted smoothing rates of nonlinear equations, such as the KPZ equation, are harder to determine analytically, but for a given starting surface they can be determined from simulations. The insets in Fig. 7 compare the measured light scattering signal during growth to the scattering signal calculated from simulations using the KPZ equation. The agreement between the calculated and measured data is quite reasonable, as the only variable parameter in the calculation is the initial amplitude. All other parameters were taken to be identical to those employed in Ref. 14 to fit the AFM images from this sample, namely, $\nu_x=10$ nm^2/s, $\nu_y=1$ nm^2/s, $\lambda_x=\lambda_y=5$ nm/s, and $\Gamma_n=10$. Most notably, the calculated time constant is only weakly q dependent (much less so than for simulations based on the linear growth equations), and is within a factor of two of both of the measured values.

During the growth of this sample, the plane of incidence of the Hg lamp lay 45° between the $[1\bar{1}0]$ and $[110]$ axes. The 16 μm^{-1} signal is measured in the plane of incidence, while the 41 μm^{-1} signal is measured at an angle 22.5° out of the plane of incidence, rotated towards the $[110]$ direction. Therefore, the 16 μm^{-1} signal measures the roughness along a direction closer to the $[1\bar{1}0]$ axis, where the value of

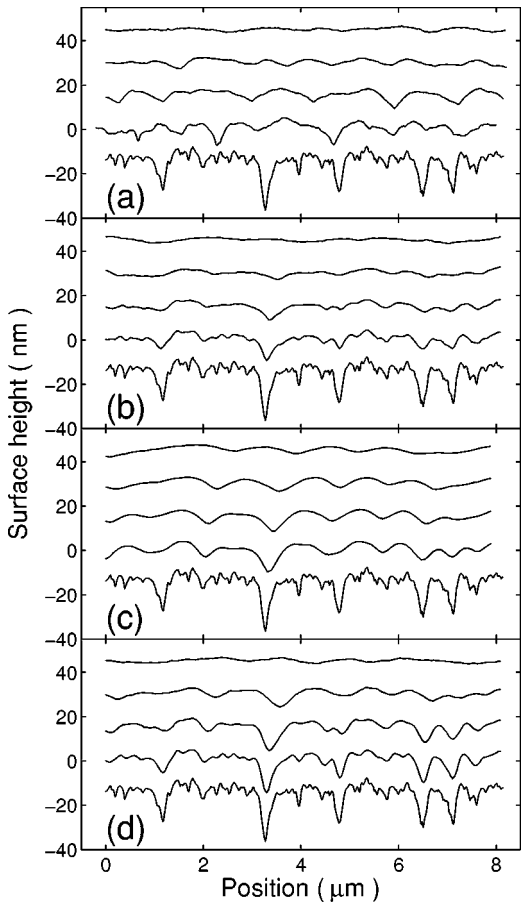

FIG. 8. Scan lines along the [110] direction from (a) measured AFM images, (b) the corresponding KPZ simulations, (c) MBE equation simulations, and (d) Edwards-Wilkinson equation simulations. From bottom to top the curves correspond to growth times of 0, 3, 10, 37.5, and 150 min. The lines in (a) are from five separate samples, whereas the scan lines in (b), (c), and (d) are taken at the same position in the evolving simulations. Scans are offset for clarity.

ν is largest, than the 41 μm^{-1} signal, which measures along a direction with a smaller value for ν. This partially offsets the expected faster smoothing rate at 41 μm^{-1}. More importantly, the KPZ term has a large effect on the smoothing rate early in the growth when the surface is at its roughest. The KPZ term tends to favor a much weaker q dependence in the smoothing rate than the linear term in the growth equation. Further simulations have shown that this weak sensitivity to length scale cannot be reproduced by the MBE equation.

Finally, in Fig. 8(a) we show a series of scan lines from AFM images of samples grown at 550 °C. From bottom to top the cross sections come from the thermally desorbed starting surface, and samples grown for 3, 10, 37.5, and 150 min (samples $T0$, $T5$, $T1$, $T2$, and $T3$, respectively). The scan lines are taken along the [110] direction and are offset by 15 nm for clarity. Figure 8(b) shows scan lines from the KPZ simulations, where the different lines are extracted at the same times as those in Fig. 8(a). Figure 8(c) shows a similar set of scan lines from the MBE equation simulations. The initial condition for the simulations is the thermally desorbed surface (sample $T0$). These lines are all taken from the same position on the surface as the simulation progressed. It is clear that while the KPZ simulations are in excellent agreement with the real surfaces at all times and length scales, the MBE equation does not correctly predict the rate at which the deepest pits fill in. This, again, indicates that the rate of change of the surface morphology during growth of this material system is only weakly q dependent.

In Fig. 8(d) we also include a series of scan lines extracted from a simulation using the Edwards-Wilkinson equation with $\nu_x = 20$ nm^2/s, $\nu_y = 5$ nm^2/s, and $\Gamma_n = 10$ (i.e., the KPZ equation with $\lambda_x = \lambda_y = 0$ nm/s). As before, the parameters have been selected to optimize the similarity between the simulated and real surfaces. Although we obtain reasonable agreement with the real data after long growth times, the large features associated with the desorption pits clearly smooth too slowly in the simulation. Furthermore, the cusplike features reproduced in the KPZ simulations become rounded in the purely linear simulation, demonstrating the importance of the nonlinear KPZ term.

2. Temperature dependence

Figure 9(a) shows an AFM scan from sample $T6$, grown for 69 min at 600 °C on a thermally desorbed substrate. The surface still shows large scale moundlike features related to the initial roughness. However, the V grooves between the mounds are not apparent, and the surface is much more inversion symmetric than the samples grown at 550 °C.

To simulate the 600 °C growth, we have scaled the linear coefficients in the KPZ equation by a factor of 3 relative to their values at 550 °C. This is the ratio that would be expected if the linear term represents a thermally activated process with activation energy of around 0.7 eV. Using values for the nonlinear coefficients of $\lambda_x = \lambda_y = 5$ nm/s, and $\Gamma_n = 10$ results in the simulation shown in Fig. 9(b). As above, the KPZ simulation generates an excellent likeness of the experimental data. The increase of the linear relative to the nonlinear coefficients enhances the anisotropy of the surface structure, and at the same time reduces the inversion asymmetry. Overall, the grown surface is smoother at 600 than at 550 °C.

B. Growth on hydrogen etched substrates

1. Kinetic roughening

Figure 10(a) shows an AFM image of a substrate from which the surface oxide has been removed by hydrogen etching. Unlike the thermal desorption process, the hydrogen etch leaves a relatively smooth surface, with an r.m.s. roughness of less than 0.2 nm in this sample. Figure 10(b) shows an AFM image from sample $H1$, grown for 75 min at 595 °C on a hydrogen etched substrate. The surface remains relatively smooth, with r.m.s. roughness equal to 0.2 nm. The large amplitude mounds seen on the thermally desorbed samples are absent in this case, but the roughness does appear to be correlated over larger length scales than on the initial substrate. A 75 min growth simulation generated using

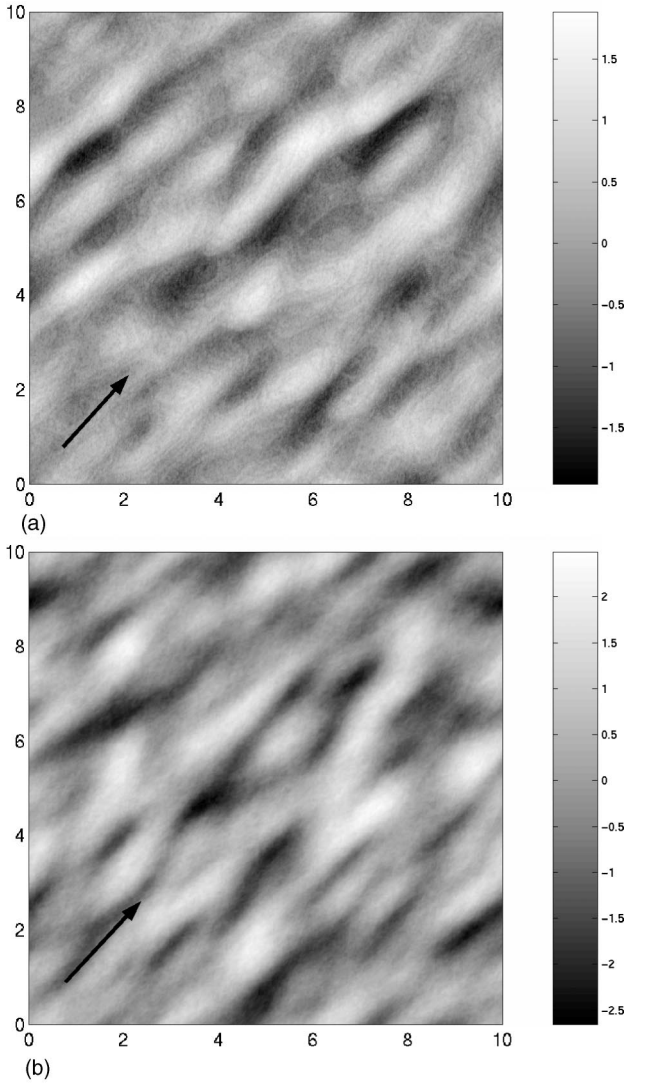

FIG. 9. (a) 10×10 μm^2 AFM image from sample $T6$, grown at 600 °C on a thermally desorbed substrate. (b) 10×10 μm^2 simulation using the KPZ equation with $\nu_x=30$ nm^2/s, $\nu_y=3$ nm^2/s, and $\lambda_x=\lambda_y=5$ nm/s. The morphology of the 600 °C grown surface is reproduced. The scale bars are in nm, and the arrows point along the $[1\bar{1}0]$ direction.

the KPZ equation with parameters $\nu_x=30$ nm^2/s, $\nu_y=3$ nm^2/s, $\lambda_x=\lambda_y=5$ nm/s, and $\Gamma_n=10$, is shown in Fig. 10(c), where the hydrogen etched surface was used as the initial condition. These parameters, which are the same as those used above to successfully model the growth at 600 °C on thermally desorbed substrates, provide an excellent likeness of the grown surface.

Because the starting surface is almost flat, we can investigate the kinetic roughening of the films grown on hydrogen etched substrates. The PSD of two such films, grown at 550 °C for 10 and 37.5 min, are shown in Figs. 11(a) and 11(b) (samples $H2$ and $H3$, respectively). The PSD of the starting surface, not shown in the figure, lies slightly below the PSD's of the grown films, and has a sharper roll-off at high spatial frequencies. In the $[1\bar{1}0]$ direction, the PSD of

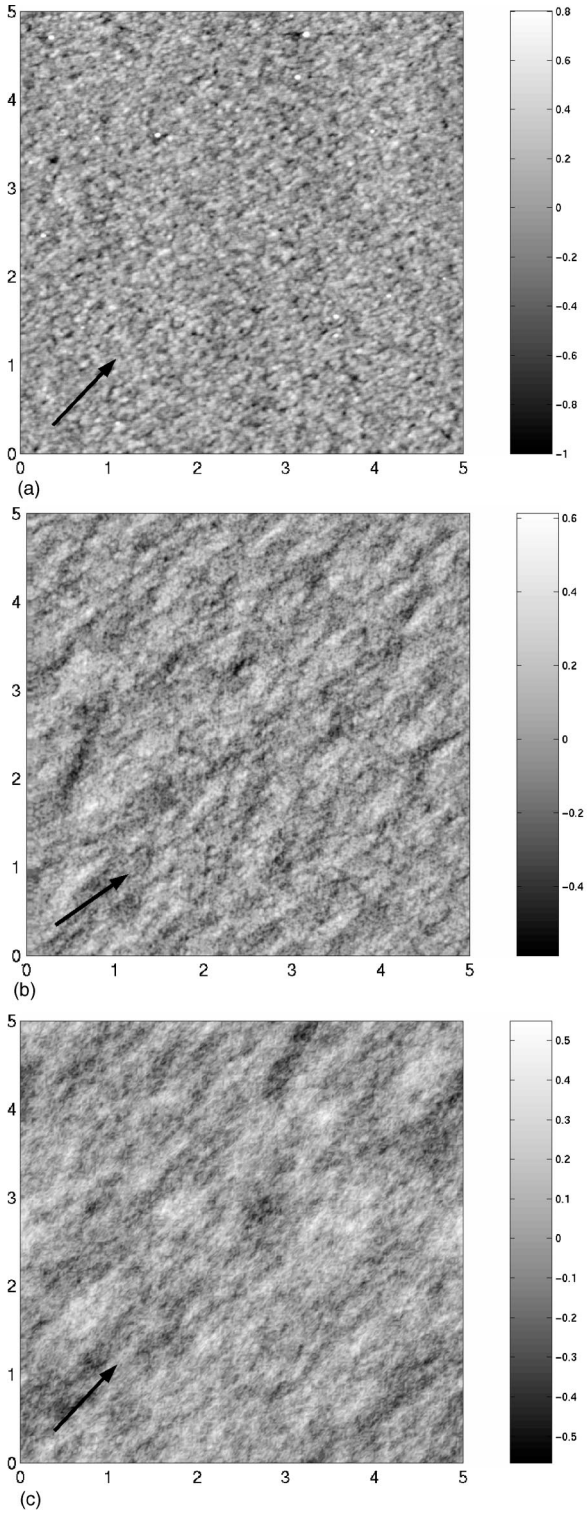

FIG. 10. (a) A 5×5 μm^2 AFM image of a GaAs wafer which has had the surface oxide removed by hydrogen etching (sample $H0$). (b) A 5×5 μm^2 AFM image from sample $H1$, grown for 75 min at 595 °C on a hydrogen etched substrate. (c) A 5×5 μm^2 simulation generated using the KPZ equation. The surface shown in (a) was used as the initial condition, and the parameters are the same as those used to simulate the growth on thermally desorbed substrates at 600 °C. The scale bars are in nm, and the arrows point along the $[1\bar{1}0]$ direction.

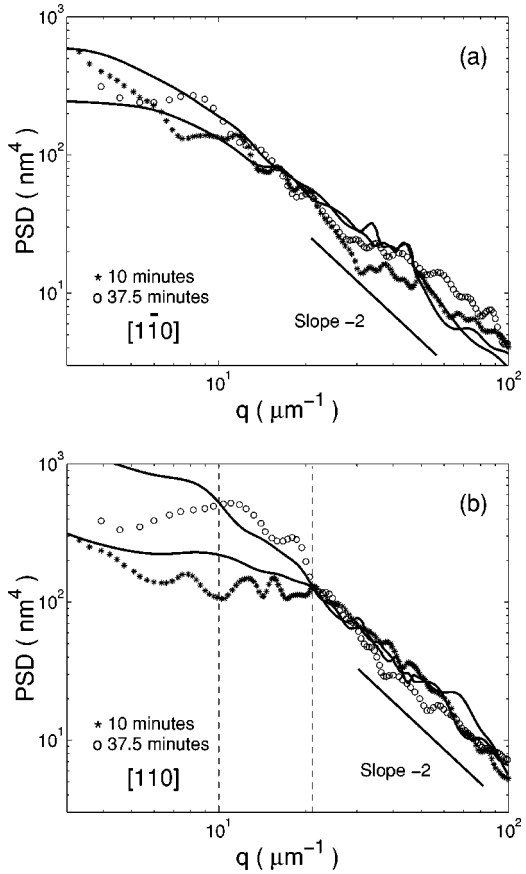

FIG. 11. PSD of samples grown on hydrogen etched substrates, measured along (a) the $[1\bar{1}0]$ direction and (b) the $[110]$ direction. The growth times are 10 and 37.5 min for samples $H2$ and $H3$, respectively. The solid lines are from simulations generated with the KPZ equation, using the same parameters used to model the growth on thermally desorbed substrates. The vertical dashed lines in (b) indicate the cutoff frequencies q_c at 10 and 37.5 min (right to left).

the grown films follows a power law with exponent approximately -2 over the entire q range. The amplitude of the PSD in this direction is independent of time, indicating that a saturated roughness has been reached. In the $[110]$ direction the PSD also follows a power law with exponent -2, but only for spatial frequencies greater than a cutoff frequency q_c of about 20 μm^{-1} after 10 min growth, and about 10 μm^{-1} after 37.5 min growth (indicated by the vertical dashed lines on the figure). Below the cutoff frequency the PSD is approximately independent of q, and has an amplitude which increases with time. This behavior is exactly what is expected from kinetic roughening; correlations develop at longer and longer length scales as time progresses, leading to a saturation in the PSD which extends to smaller and smaller spatial frequencies. The PSD saturates more quickly along the $[1\bar{1}0]$ axis due to the more rapid smoothing rate in this direction.

The solid lines in Figs. 11(a) and 11(b) show simulated PSDs generated with the KPZ equation using the same parameters used to generate the simulated PSDs in Figs. 5(a) and 5(b), but with a hydrogen etched starting surface. The simulations are in excellent agreement with the measured data. Most notably, the slope and amplitude of the saturated PSD's are reproduced, and the position of the cutoff frequency q_c is in good agreement with the data. Therefore, we conclude that the modified KPZ equation describes the growth on both smooth and rough initial surfaces.

The exponent of the power law describing both the measured and the simulated PSD's is close to -2 in both directions. This is in agreement with the exponents measured on the thermally desorbed surfaces, although it is somewhat surprising, as it differs from the KPZ prediction of -2.8. We return to this point in Sec. V, below.

2. Dependence on As overpressure

The anisotropy of the surface structure is sensitive to the As_2 overpressure during growth. This is demonstrated in Fig. 12 which shows three high resolution AFM scans from samples grown at 550 °C on hydrogen etched substrates under varying As_2 flux [samples $H3$ (a), $H4$ (b), and $H5$ (c)]. Well defined atomic steps are visible in all three images. At a group V to group III flux ratio of 6.5 [Fig. 12(a)] the surface is covered with islands which show a moderate amount of elongation along the $[1\bar{1}0]$ direction, as demonstrated by the relatively isotropic two dimensional PSD shown in the inset. As the V:III ratio is decreased to 3.0 [Fig. 12(b)] the anisotropy increases, and the PSD becomes much more elongated. In terms of the continuum growth equations this corresponds to an enhancement in the anisotropy of the coefficients. Physically, the elongation results from an anisotropic mobility of the adatoms, and possibly also an anisotropy in the incorporation dynamics on the surface.[27] Due to the 2×4 surface reconstruction some degree of anisotropy is present even at the highest As flux. Once the V:III ratio approaches unity [Fig. 12(c)] the surface structure changes considerably, possibly due to an imminent change in the reconstruction from 2×4 to 2×2. The surface is now covered by terraces that are almost continuous along the $[1\bar{1}0]$ direction, each with a characteristic width of around 80 nm. This length scale is reflected in the PSD, which now shows two peaks on either side of the origin along the direction of elongation.

The GaAs surfaces described in Refs. 8–10, on which mounds were attributed to unstable growth, also show a large degree of anisotropy. This indicates that they were grown under an effectively lower As overpressure (As_4 was used as the source) than most of the samples displayed here. It is therefore interesting to consider whether an appreciable Ehrlich-Schwoebel barrier may exist in conditions of low As flux. The length scale in Fig. 12(c) could be taken as indicating the presence of an Ehrlich-Schwoebel barrier in the $[110]$ direction, but we note that the tops of the terraces are almost atomically flat, whereas in unstable growth sloped terraces would be expected. The exact mechanism by which this surface morphology forms is unknown, but it does not appear to be easy to model with continuum growth equations, either stable or unstable.

V. DISCUSSION

The simulations show that both the KPZ and the MBE equation can qualitatively reproduce the mounds on the sur-

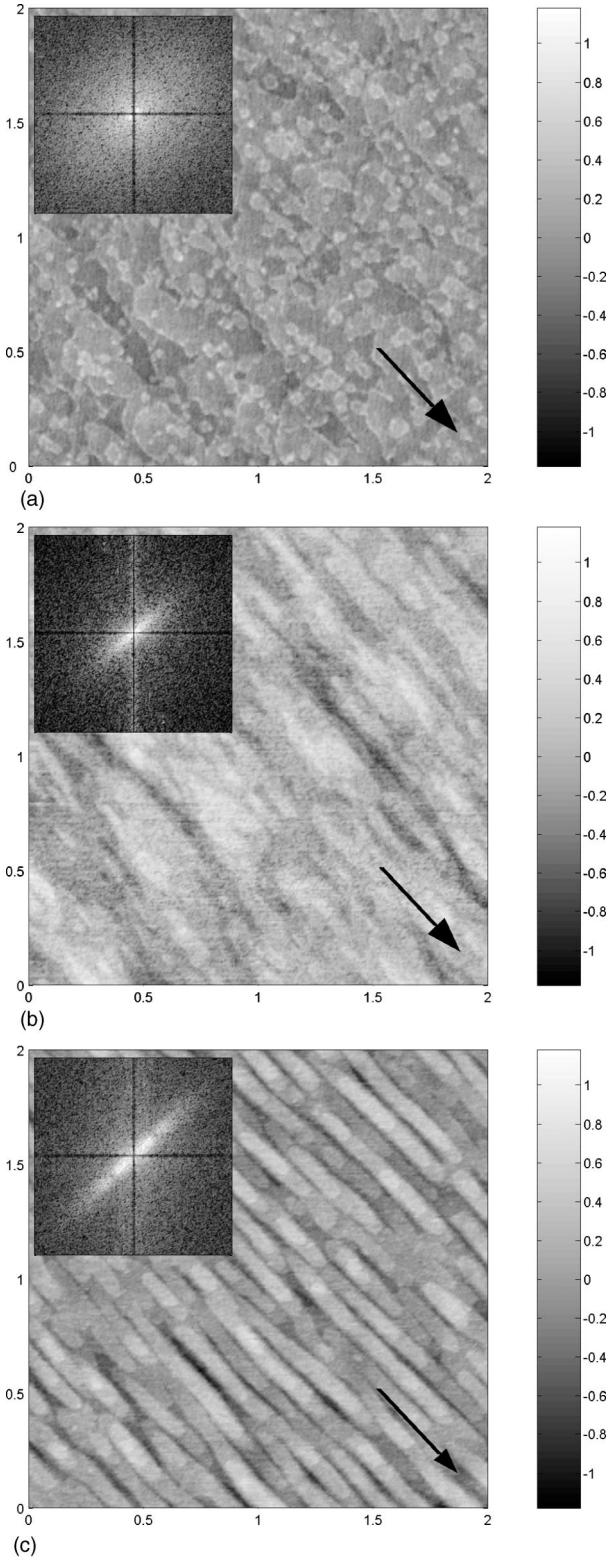

FIG. 12. 2×2 μm^2 AFM images illustrating the effect of reducing the As_2 overpressure. (a) V:III ratio=6.5 (sample $H3$), (b) V:III ratio=3.0 (sample $H4$), and (c) V:III ratio=1.0 (sample $H5$). The scale bars are in nm, and the surface features are elongated along the $[1\bar{1}0]$ direction (along the arrow). The 2D PSD of each image is included as an inset, with spatial frequencies ranging from -300 to 300 μm^{-1} in each direction.

face. Quantitatively, however, only the KPZ equation is able to reproduce the PSD of the surfaces. This is because the measured PSD smooths at a rate which is fairly insensitive to the length scale being probed. The stronger spatial frequency dependence inherent in the higher order MBE equation makes it difficult to reproduce the relatively q independent decrease in the measured PSD (see Figs. 5 and 6).

It is important, then, to consider the physical origin of the terms in the KPZ equation, as it applies to GaAs homoepitaxy. To gain insight, we have compared high resolution AFM images of samples which were annealed at growth temperature for 15 min after completion of the film, with samples which were quenched in temperature immediately after growth.[28] For films grown under similar conditions, the large scale surface morphology of the annealed and unannealed samples is very similar. However, at short length scales smooth atomic terraces are far more pronounced on the annealed samples, while the terraces in the quenched samples are made up of a large density of small islands. Clearly the small islands coalesce into smooth terraces during annealing. This indicates that Ga atoms attached to step edges are able to dissociate from the step and return to the mobile adatom phase under MBE conditions. A single Ga atom may therefore make several visits to step edge sites on the surface before finally being incorporated into the film. This is consistent with the growth process being dominated by an evaporation/condensation like dynamics between the surface and the adatoms. As discussed in Sec. II A, the second order linear term in the growth equation then arises from the leading $\nabla^2 h$ term in an expansion of the surface chemical potential.

The values of λ required in the simulations are considerably larger than the growth rate of around 0.3 nm/s, so the nonlinear KPZ term cannot be accounted for by simply assuming the surface grows outward from the surface normal. Instead, we believe the KPZ term represents a correction to the surface chemical potential due to the incident flux. This $(\nabla h)^2$ correction has been discussed in the context of the fourth order MBE equation.[1,17] In our case, the rate limiting step in the smoothing of the surface appears to be the incorporation of adatoms at sites with low chemical potential, rather than the diffusion of adatoms driven by gradients in the chemical potential. Therefore, the nonlinearity is of second order rather than fourth order.

Our interpretation of the terms in the KPZ equation also provides a natural explanation for the excess noise in the KPZ simulations. The noise represents fluctuations in the density of adatoms at a given point on the surface. When adatoms are both incorporating and dissociating from step edges, these fluctuations can easily be much larger than the fluctuations in the arrival rate of adatoms from the flux. Furthermore, due to the existence of the 2×4 surface reconstruction, it may not be favorable for Ga adatoms to incorporate individually.[27] Instead, the basic unit which must be added to the surface may consist of several Ga atoms, for example, enough to recreate a unit cell of the 2×4 reconstruction. In this case the coefficient of the noise correlation function will be modified from $D=Fa^3$ to $D=nFa^3$, where n is the number of Ga atoms forming the basic incorporation

unit. Therefore the value $\Gamma_n = 10$ used in the KPZ simulations seems entirely reasonable.

We now comment on the power law observed in the PSD at high spatial frequencies. Despite the importance of the nonlinear terms for reproducing the surface morphology, the PSD tends to display the power law exponent expected for the purely linear equations (i.e., -2). This should not be taken as indicating a disagreement with the theoretical predictions. Instead, it simply indicates that we are in a transient regime in which the relatively large linear terms are dominating the nonlinear terms at short length scales.[22] The small surface roughness at short length scales means that the nonlinear term can be neglected in this regime. This conclusion is supported by the results of further simulations using the KPZ equation. For example, using the isotropic parameters $\nu = 5$ nm^2/s, $\lambda = 5$ nm/s, and $\Gamma_n = 10$ the simulations exhibit a power law exponent of -2 in the PSD even after 1000 min of growth on a flat 10×10 μm^2 substrate. However, using the parameters $\nu = 0.01$ nm^2/s, $\lambda = 5$ nm/s, and $\Gamma_n = 10$ an exponent of -2.8 is observed for times greater than about 60 min.

VI. CONCLUSIONS

Based on our comparison between experimental data and simulations of continuum growth equations, we conclude that the evolution of the surface morphology of MBE grown GaAs is described by the KPZ equation with a stable linear term. By contrast, the MBE equation fails to reproduce the measured surface morphology of the grown films. These results lead us to the following interpretation of the dominant smoothing mechanism during film growth. The surface is covered by mobile adatoms which diffuse randomly on the surface, forming an effective vapor phase. Incorporation of these adatoms takes place preferentially at sites on the surface with positive curvature, as described by a second order growth equation. Nonlinear corrections to the incorporation rate are observed to be important. We attribute these corrections to a noneqilibrium contribution to the surface chemical potential associated with the deposition flux. Mass transport driven by gradients in the surface chemical potential, as described by the MBE equation, does not appear to play a significant role, being dominated instead by the incorporation dynamics. In MBE growth, the incorporation process must necessarily be of a conservative nature, i.e., the growth rate should not depend on the surface slope. To account for this fact we have made a slight correction to the KPZ equation. It is important to point out that, due to the rather small slopes on even the thermally desorbed substrates, this modification has only a very minor effect on the morphology of the simulated surfaces. Therefore, the simulations are essentially indistinguishable from simulations of the unmodified KPZ equation.

For a given growth condition, a single set of parameters successfully describes growth on surfaces with different initial roughness, demonstrating the applicability of the KPZ equation. Regardless of initial condition, after long growth times the surface tends towards an equilibrium roughness level determined by the interplay between the smoothing rate and random noise in the system, as predicted by kinetic roughening theory. We have found that increasing the temperature or As overpressure leads to smoother surfaces, implying increased values for the coefficients of the smoothing terms in the KPZ equation. Increasing the As overpressure also reduces the anisotropy of the surface morphology.

ACKNOWLEDGMENTS

We thank B. Bergersen and M. Plischke for useful discussions, and NSERC and the BC Science Council (M.A.) for financial assistance.

APPENDIX NUMERICAL METHOD

Conventional finite difference schemes for the nonlinear term in the KPZ equation use a centered difference approximation, such as $(\nabla h)^2 \approx (h_{i+1} - h_{i-1})^2 / 4\Delta x^2$, where h_i is the height at the ith point on the one-dimensional (1D) surface, and Δx is the spacing between the points. As noted in Ref. 22, this implementation fails to include the grid point h_i, and can be highly unstable. This restricts the range of parameters which can be used in simulations, so instead we have used an alternate implementation based on the normal growth interpretation of the KPZ term [Eq. (3)], where the surface is translated outwards from the local surface normal by a constant amount.

Consider the 1D discrete representation of a surface shown in Fig. 13(a). The dashed lines show the positions of each surface element after translation outwards by a uniform amount. The thick solid line shows the new surface generated from the dashed lines, by choosing the maximum at any point where there is ambiguity in the choice of the new height. This procedure can be generalized to 2D. Figure 13(b) shows the stencil used for the 2D calculation, where the relevant surface elements have been shaded. At most only one of the four shaded surface elements will actually decide the final height increment at point P. To determine which this is, we find the largest of h_A, h_B, h_C, and h_D, and call this h_1. Of the two remaining points of A, B, C, and D which are closest to this point, we find the one with the next largest h, and call this h_2. Then, assuming $\Delta x = \Delta y$,

$$\Delta h_P = \begin{cases} \lambda\, dt, & \text{if } [h_1 \leqslant h_P \,\&\, h_2 \leqslant h_P], \\ \lambda\, dt \sqrt{1 + [(h_P - h_1)/\Delta x]^2}, & \text{if } [h_1 > h_P \,\&\, h_2 \leqslant h_P], \\ \lambda\, dt \sqrt{1 + [(h_P - h_1)/\Delta x]^2 + [(h_P - h_2)/\Delta x]^2}, & \text{if } [h_1 > h_P \,\&\, h_2 > h_P]. \end{cases} \tag{A1}$$

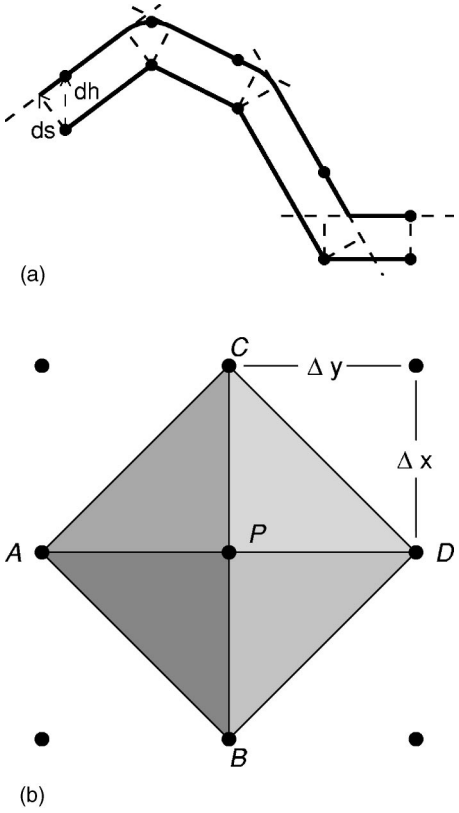

FIG. 13. (a) Application of the normal growth algorithm to a discrete representation of a 1D surface. The surface is translated outwards by an amount $ds=\lambda dt$, leading to a growth rate in the vertical direction of dh. (b) The 2D stencil $[ABCDP]$ used to calculate the $(\nabla h)^2$ term at point P.

The final step is to subtract λdt from the matrix of height increments, thus leaving a matrix of values closely approximating $\lambda(\nabla h)^2/2$. This algorithm is stable for any values of λ, as long as the time step is not excessive. Furthermore, the simulation code can be fully vectorized, leading to a 16-fold decrease in calculation time over an implementation using nested for loops to access the matrix elements. The algorithm has been fully tested on artificial surfaces for which $(\nabla h)^2$ can be calculated exactly.

The conservative form of the KPZ equation [Eq. (5)] is implemented via an extension to the nonconservative KPZ simulation. After calculating Δh on an $N\times N$ matrix for a given time step using Eq. (A1), the total volume represented by Δh is determined: $dV=\Sigma\Delta x^2\Delta h$. This is done prior to subtracting λdt from Δh. The new matrix Δh_C is then calculated: $\Delta h_C=\Delta h(dV/dV_0)-\lambda dt$, where $dV_0=\lambda(N\Delta x)^2$ is the volume that would be added to a flat surface during the same time step using the growth rule Eq. (A1). Note that this is not the same as ensuring a conservative growth term by simply subtracting the average surface height at each time step.

The second order linear term is implemented using a five point stencil on the 2D lattice, i.e.,

$$\nabla^2 h \approx \nu_x\left[\frac{h_{i+1,j}-2h_{i,j}+h_{i-1,j}}{\Delta x^2}\right] + \nu_y\left[\frac{h_{i,j+1}-2h_{i,j}+h_{i,j-1}}{\Delta y^2}\right], \tag{A2}$$

where $\Delta x=\Delta y$ in our simulations. The fourth order linear term is implemented with a nine point stencil as

$$\nabla^4 h \approx \kappa_x\left[\frac{h_{i+2,j}-4h_{i+1,j}+6h_{i,j}-4h_{i-1,j}+h_{i-2,j}}{\Delta x^4}\right] + \kappa_y\left[\frac{h_{i,j+2}-4h_{i,j+1}+6h_{i,j}-4h_{i,j-1}+h_{i,j-2}}{\Delta y^4}\right]. \tag{A3}$$

The different coefficients $(\nu_x,\nu_y,\kappa_x,\kappa_y)$ allow for the inclusion of anisotropy in the simulations. Linear transformations of the terms in the numerical calculation allow the anisotropy axis to be rotated such that they match the elongation axis of the AFM images. It is obvious from Eq. (2) that this algorithm can also be used to simulate the fourth order nonlinear term, by simply applying the ∇^2 scheme to the matrix of $(\nabla h)^2$ values generated in the manner described above.

*E-mail address: anders@physics.ubc.ca; web address: URL http://www.physics.ubc.ca/~mbelab/
†Present address: School of Chemical and Physical Sciences, Victoria University of Wellington, New Zealand.
‡Present address: Department of Physics, Cambridge University, Cambridge, United Kingdom.

[1] J. Krug, Adv. Phys. **46**, 139 (1997).
[2] A. -L. Barabási and H. E. Stanley, *Fractal Concepts in Surface Growth* (Cambridge University Press, Cambridge, UK, 1995).
[3] A. Pimpinelli and J. Villain, *Physics of Crystal Growth* (Cambridge University Press, Cambridge, UK, 1998).
[4] T. Halpin-Healy and Y.-C. Zhang, Phys. Rep. **254**, 215 (1995).
[5] G. Ehrlich and F.G. Hudda, J. Chem. Phys. **44**, 1039 (1966).
[6] R.L. Schwoebel and E.J. Shipsey, J. Appl. Phys. **37**, 3682 (1966).
[7] G. Apostolopoulos, J. Herfort, L. Däweritz, K.H. Ploog, and M. Luysberg, Phys. Rev. Lett. **84**, 3358 (2000).
[8] A.W. Hunt, C. Orme, D.R.M. Williams, B.G. Orr, and L.M. Sander, Europhys. Lett. **27**, 611 (1994).
[9] M.D. Johnson, C. Orme, A.W. Hunt, D. Graff, J. Sudijono, L.M. Sander, and B.G. Orr, Phys. Rev. Lett. **72**, 116 (1994).
[10] C. Orme, M.D. Johnson, J.L. Sudijono, K.T. Leung, and B.G. Orr, Appl. Phys. Lett. **64**, 860 (1994).
[11] V.R. Coluci, M.A. Cotta, C.A.C. Mendonça, K.M.I. -Landers, and M.M.G. de Carvalho, Phys. Rev. B **58**, 1947 (1998).
[12] V.R. Coluci and M.A. Cotta, Phys. Rev. B **61**, 13 703 (2000).
[13] M. Kardar, G. Parisi, and Y.-C. Zhang, Phys. Rev. Lett. **56**, 889 (1986).
[14] A. Ballestad, B.J. Ruck, M. Adamcyk, T. Pinnington, and T. Tiedje, Phys. Rev. Lett. **86**, 2377 (2001).
[15] T. Sun, H. Guo, and M. Grant, Phys. Rev. A **40**, 6763 (1989).

[16] D.E. Wolf and J. Villain, Europhys. Lett. **13**, 389 (1990).
[17] Z.-W. Lai and S. Das Sarma, Phys. Rev. Lett. **66**, 2348 (1991).
[18] S.F. Edwards and D.R. Wilkinson, Proc. R. Soc. London, Ser. A **381**, 17 (1982).
[19] S. Das Sarma, Fractals **1**, 784 (1993).
[20] S. Das Sarma and R. Kotlyar, Phys. Rev. E **50**, R4275 (1994).
[21] W.W. Mullins, J. Appl. Phys. **28**, 333 (1957).
[22] T.J. Newman and A.J. Bray, J. Phys. A **29**, 7917 (1996).
[23] S.R. Johnson, C. Lavoie, T. Tiedje, and J.A. Mackenzie, J. Vac. Sci. Technol. B **11**, 1007 (1993).
[24] E.L. Church, H.A. Jenkinson, and J.M. Zavada, Opt. Eng. **18**, 125 (1979).
[25] M. Adamcyk, A. Ballestad, T. Pinnington, T. Tiedje, M. Davies, and Y. Feng, J. Vac. Sci. Technol. B **18**, 1488 (2000).
[26] T. H. Pinnington, Ph. D. thesis, University of British Columbia, 1994.
[27] M. Itoh, Phys. Rev. B **64**, 045301 (2001).
[28] A. Ballestad, B.J. Ruck, J.H. Schmid, and T. Tiedje (unpublished).